chemosensors

MDPI

Article

Highly Selective Recognition of Pyrophosphate by a Novel Coumarin-Iron (III) Complex and the Application in Living Cells

Wei Wang [1], Hongren Zhao [1], Bing Zhao [2], Huimin Liu [1], Qinglei Liu [1] and Yan Gao [3,*]

[1] School of Perfume and Aroma Technology, Shanghai Institute of Technology, Shanghai 201418, China; wangweittg@sit.edu.cn (W.W.); zhaohongren2021@163.com (H.Z.); szliuhm@163.com (H.L.); liuqinglei2006888@163.com (Q.L.)
[2] Chemistry and Chemical Engineering Institute, Qiqihar University, Qiqihar 161006, China; zhao_submit@aliyun.com
[3] School of Chemical Engineering, University of Science and Technology Liaoning, Anshan 114051, China
* Correspondence: gys20080901@163.com; Tel.: +86-130-5004-8886

Abstract: In this paper, a novel **NL**-Fe^{3+} ensemble was designed as a fluorescent chemosensor for highly selective detection of pyrophosphate (PPi) in DMSO/H_2O (2:8/*v*:*v*, pH = 7.2) solution and living cells. **NL** showed a strong affinity for Fe^{3+} and was accompanied by obvious fluorescence quenching. Upon the addition of PPi to the generated **NL**-Fe^{3+} ensemble, the fluorescence and absorption spectra were recovered completely. Spectroscopic investigation showed that the interference provoked by common anions such as adenosine-triphosphate (ATP), adenosine diphosphate (ADP), and phosphates (Pi) can be ignored. The detection limit of **NL**-Fe^{3+} to PPi was calculated to be 1.45×10^{-8} M. Intracellular imaging showed that **NL**-Fe^{3+} has good membrane permeability and could be used for the detection of PPi in living cells. A B3LYP/6-31G(d,p) basis set was used to optimize **NL** and **NL**-Fe^{3+} complex.

Keywords: coumarin; Fe(III); pyrophosphate; cells imaging

Citation: Wang, W.; Zhao, H.; Zhao, B.; Liu, H.; Liu, Q.; Gao, Y. Highly Selective Recognition of Pyrophosphate by a Novel Coumarin-Iron (III) Complex and the Application in Living Cells. *Chemosensors* **2021**, *9*, 48. https://doi.org/10.3390/chemosensors9030048

Academic Editor: Moustafa Gabr

Received: 20 January 2021
Accepted: 24 February 2021
Published: 28 February 2021

1. Introduction

Phosphates and their derivatives play an important role in the process of building the most fundamental molecules in living organisms. As we know, DNA and RNA make up the main macromolecules necessary for all known life. Phosphates are also a major ingredient of lipid membranes and are involved in many biological processes, which include skeletal development and integrity, cell sensing, and regulation of protein synthesis [1,2]. The change of PPi concentration in biological environments can be used as a diagnostic indicator for various clinical conditions. For example, crystal deposition of calcium pyrophosphate dehydration (CPPD) may result in abnormally high levels of PPi in synovial fluid [3,4], the level of intracellular PPi can provide important information about cellular processes for cancer diagnosis [5]. The fluctuations in PPi concentration in physiological fluids such as synovial fluid and urine can also be used to identify series of diseases such as chondrocalcification and so on [6]. Therefore, the identification of PPi has become a very important research hotspot.

Among various methods for detecting anions, anion-selective fluorescent probes have attracted more and more attention because of their high sensitivity and easy-to-operate features [7,8]. Numerous probes for detecting anions have been devised and are based on hydrogen bonding, anion-π interactions, and metal-anion chelation [9–11]. Of these, metal complex chemosensors have been reported for the detection of anions because the coordination flexibility of metal centers can provide a good way for organizing anion binding groups. These complexes are usually not fluorescent due to metal-ion-induced fluorescence quenching. By virtue of the high affinity between metal and anion, the metal

ion is detached from the complex in the presence of anion, switching on fluorescence for quantitative detection [12–15]. Over the past few years, many excellent fluorescent chemosensors for PPi have been reported. However, there are relatively few chemosensors for detecting PPi in aqueous media and biological systems reported to date [16–18], which are also not free from disadvantages such as low sensitivity, slow response time, interference from ATP, ADP, and so on [19]. Recently, based on the displacement strategy, we reported a Fe^{3+}-based chemosensor for detecting PPi in DMSO/H_2O (3:7/*v*:*v*, pH = 7.2) solution [20], which showed good selectivity and sensitivity to PPi, and the interference caused by other common anions such as ATP, ADP, and Pi is low or not relevant. However, there is still a demand to develop homogeneous PPi sensing systems that are selective over di- and trinucleoside phosphates.

In this work, considering the flexible coordination way of heteroatoms-metal ion and the excellent fluorescence properties of coumarin, a novel coumarin-based fluorescent ligand, **NL**, was synthesized and characterized (Scheme 1). After the complexation of **NL** with Fe^{3+}, the **NL**-Fe^{3+} complex showed no fluorescence owing to the paramagnetic quenching effect of Fe^{3+}. In the presence of PPi, the resultant **NL**-Fe^{3+} complex is switched on upon addition of PPi due to the high affinity of Fe^{3+} to PPi. The detection limit of **NL**-Fe^{3+} to PPi was determined to be 1.45×10^{-8} M. This "OFF-ON" fluorescence identification can provide a convenient approach for the detection of PPi in biological samples (Scheme 2).

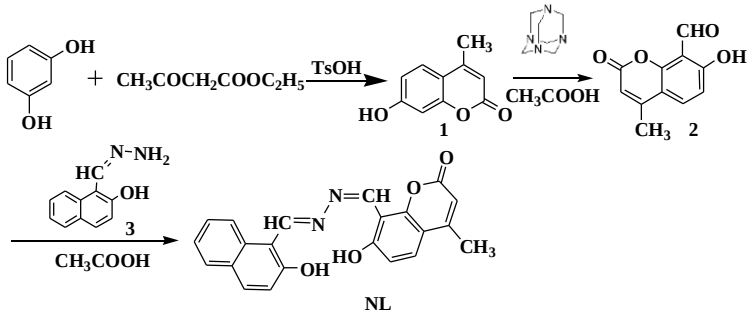

Scheme 1. Synthesis of fluorescence chemosensor **NL**.

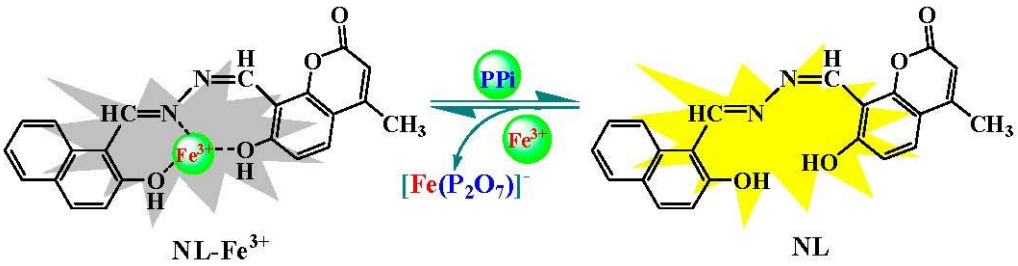

Scheme 2. Proposed response mechanism of **NL**-Fe^{3+} towards pyrophosphate (PPi).

2. Materials and Methods

2.1. Apparatus and Reagents

UV-Vis and fluorescence spectra were measured on a Lambda-900 spectrometer and Perkin-Elmer LS-55 fluorescence spectrophotometer (Perkin-Elmer, Waltham, MA, USA). ^{1}H NMR and ^{13}C NMR (internal standard TMS) were recorded on a Bruker 500 and 125 MHz spectrometers (Karlsruhe, Germany), respectively. Mass spectrometry was performed with a Bruker Solari X70 high-resolution mass spectrometer (Bruker, Karlsruhe, Germany). The elemental analysis was tested using a Perkin-Elmer 240 microanalyzer (PerkinElmer, Waltham, MA, USA).

All chemical reagents were purchased from Aladdin Reagents Company (Shanghai, China). The solvents used for synthesis and spectroscopic studies were analytic grade and

spectroscopic grade reagent. Water was double distilled and all metal salts except ferric chloride and zinc chloride are nitrates in the experiments.

2.2. Synthesis of Compound NL

The synthetic route of probe **NL** is shown in Scheme 1, 4-methyl-7-hydroxy coumarin **1**, 7-hydroxy-4-formyl coumarin **2**, and naphthalene hydrazine **3** were prepared according to reported procedures [21,22]. A mixture of intermediates **2** (3 mmol) and **3** (3 mmol) were dissolved in 25 mL of acetic acid and refluxed until complete reaction of raw material. An orange precipitate appeared in the process of reaction; the filtered crude was purified by column chromatography to obtain a yellow solid **NL** (yield: 56%). ^{1}H NMR (500 MHz, DMSO-d_6) δ(ppm): 12.56 (s, 1H), 12.51 (s, 1H), 9.97 (d, J = 10.4 Hz, 1H), 9.33 (s, 1H), 8.64 (d, J = 8.2 Hz, 1H), 8.02 (d, J = 8.5 Hz, 1H), 7.89 (d, J = 8.2 Hz, 1H), 7.77 (d, J = 8.8 Hz, 1H), 7.64–7.57 (m, 1H), 7.42 (t, J = 7.3 Hz, 1H), 7.24 (d, J = 8.4 Hz, 1H), 7.00 (d, J = 8.6 Hz, 1H), 6.26 (s, 1H), 2.39 (s, 3H). ^{13}C NMR (125 MHz, DMSO-d_6) δ(ppm): 162.8, 161.9, 160.2, 158.9, 157.3, 153.6, 135.1, 132.2, 129.7, 128.7, 128.0, 127.7, 123.7, 121.9, 118.7, 118.6, 113.3, 111.8, 110.7, 108.2, 105.2, 18.1. FT-MS, m/z: 373.11879 ($M+H^+$); Anal. Calcd for $C_{22}H_{16}N_2O_4$: C, 70.96; H, 4.33; N, 7.52. Found: C, 70.91; H, 4.35; N, 7.56.

2.3. Synthesis of NL-Fe^{3+} Complex

Ligand **NL** (0.5 mmol) and ferric chloride (0.6 mmol) were dissolved in acetonitrile (20 mL). The resulting suspension was heated under reflux for 5 h until a green precipitate formed. It was filtered off while hot, washed with Et_2O, and dried in vacuo. The solid obtained was filtered and recrystallized from ethanol to afford a green solid. FT-IR (cm^{-1}): 3433 (OH), 2919 (CH), 1545 (C=N), 845 (C–Cl), 542 (Fe–N), 457 (Fe–O). FT-MS, m/z: 498.94274; Anal. Calcd for $C_{22}H_{16}Cl_2FeN_2O_4$: C, 52.96; H, 3.23; N, 5.61; Cl, 14.21. Found: C, 52.91; H, 3.24; N, 5.63; Cl, 14.24. Conductivity:109 $S{\cdot}cm^{-1}{\cdot}mole^{-1}$.

2.4. Computational Details

Density functional theory (DFT) method was used to optimize the geometry and electronic structures of **NL** and **NL**-Fe^{3+} at the B3LYP/6-311+G (d,p) level by using Gaussian 09 software [23].

2.5. Calculation of Association Constant

The association constant of **NL**-Fe^{3+} was calculated using the Benesi–Hildebrand (B–H) plot (Equation (1)) [24].

$$1/(F_0 - F) = 1/\{K_a\,(F_0 - F_{min})\,C\} + 1/(F_0 - F_{min}) \quad (1)$$

where F_0 and F are the fluorescence intensity of **NL** and the emission intensity in the presence of analyte with different concentrations, respectively; F_{min} is the minimum emission intensity value obtained by fluorescence titration; and K_a is the association constant and was determined by the slope of the linear plot.

2.6. Cytotoxicity Assays

Hela cells were cultured in Dulbecco's Modified Eagle Medium (DMEM) in an atmosphere of 5% CO_2 and 95% air at 37 °C for 24 h, and then 0–30 μM **NL** dissolved in DMSO/H_2O solution (2:8/*v*:*v*) was added. Then, the labeled cells were cultured in the same environment for 48 h. Finally, 20 mL of 3-(4,5-dimethylthiazole-2-yl)-2,5-diphenyltetrabromazole (MTT) was added and cultured for 6 h.

3. Results and Discussion

3.1. Synthesis and Spectroscopic Characterization of the NL-Fe^{3+}

NL and **NL**-Fe^{3+} complex were characterized by ^{1}H NMR, ^{13}C NMR, FT-MS, IR, and elemental analysis (Figures S1–S6, Supplementary materials). The stability of **NL** was

studied in DMSO/H_2O (2:8/*v*:*v*, pH = 7.2) solution. As shown in Figure S9, the fluorescence of **NL** (10 μM) did not change significantly within 24 h, which showed that **NL** was stable under experimental conditions. Then, 1.0 equivalent of $FeCl_3$ was added to **NL** (10 μM) solution to prepare the stock solution of **NL**-Fe^{3+} for detecting PPi. The complexation behavior of **NL** with Fe^{3+} was investigated by a fluorescence titration experiment. The ligand **NL** has a strong emission at 557 nm when the excitation wavelength is 410 nm, the fluorescence intensity of **NL** was gradually quenched with the increase of Fe^{3+} concentration (0–2 equiv.) (Figure 1A), and the emission color of the solution changed from yellow to colorless under the ultraviolet lamp (Figure 1A inset), indicating a complete formation of **NL**-Fe^{3+} complex [25]. A remarkable fluorescence quenching (quenching efficiency at 557 nm, $(I_0 - I)/I_0 \times 100\%$ = 86 %) is observed in the presence of 10 μM Fe^{3+} (Figure S10). However, **NL** had no obvious fluorescence response upon the addition of other metal ions such as Cr^{3+}, Cu^{2+}, Ag^{+}, Co^{2+}, K^{+}, Hg^{2+}, Pb^{2+}, Ba^{2+}, Ni^{2+}, Mg^{2+}, Cd^{2+}, Ca^{2+}, Zn^{2+}, Al^{3+}, and Na^{+} (Figure 1B).

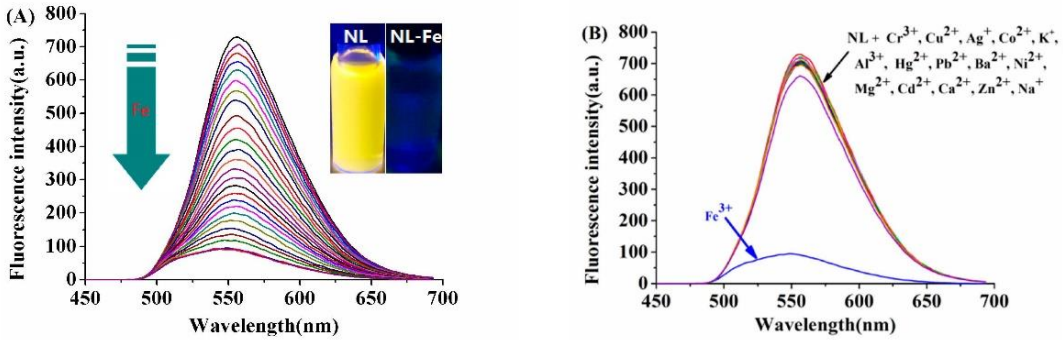

Figure 1. (**A**) Fluorescence titration of **NL** (10 μM) in the presence of different amounts of Fe^{3+} (0–20 μM) in DMSO/H_2O (2:8/*v*:*v*, 20 mM HEPES, pH = 7.2) solution. Inset: Changes in fluorescence color of **NL** (10 μM) upon the addition of Fe^{3+} (10 μM). (**B**) Fluorescence responses of **NL** (10 μM) to different cations (20 μM): Cr^{3+}, Cu^{2+}, Ag^{+}, Co^{2+}, K^{+}, Hg^{2+}, Pb^{2+}, Fe^{3+}, Ba^{2+}, Ni^{2+}, Mg^{2+}, Cd^{2+}, Ca^{2+}, Zn^{2+}, Al^{3+}, and Na^{+}.

In addition, potential interferences were investigated by adding Fe^{3+} to the mixture of **NL** and multiple coexisting cations. As shown in the Figure S11, the quenching effect induced by Fe^{3+} was not interfered with by other competitive cations, indicating that **NL** has high specificity for Fe^{3+} binding. The complexation stoichiometry of **NL**-Fe^{3+} was determined by Job plot; the results showed that **NL** coordinates to Fe^{3+} to form a complex in 1:1 stoichiometry (Figure 2A) [26]. According to Benesi–Hildebrand equation, the intensity $(1/(F_0-F))$ of **NL** changed linearly with $1/[Fe^{3+}]$ (R^2 = 0.9949), and the association constant of **NL** with Fe^{3+} was calculated to be 2.29 × 10^5 M^{-1}(Figure 2B).

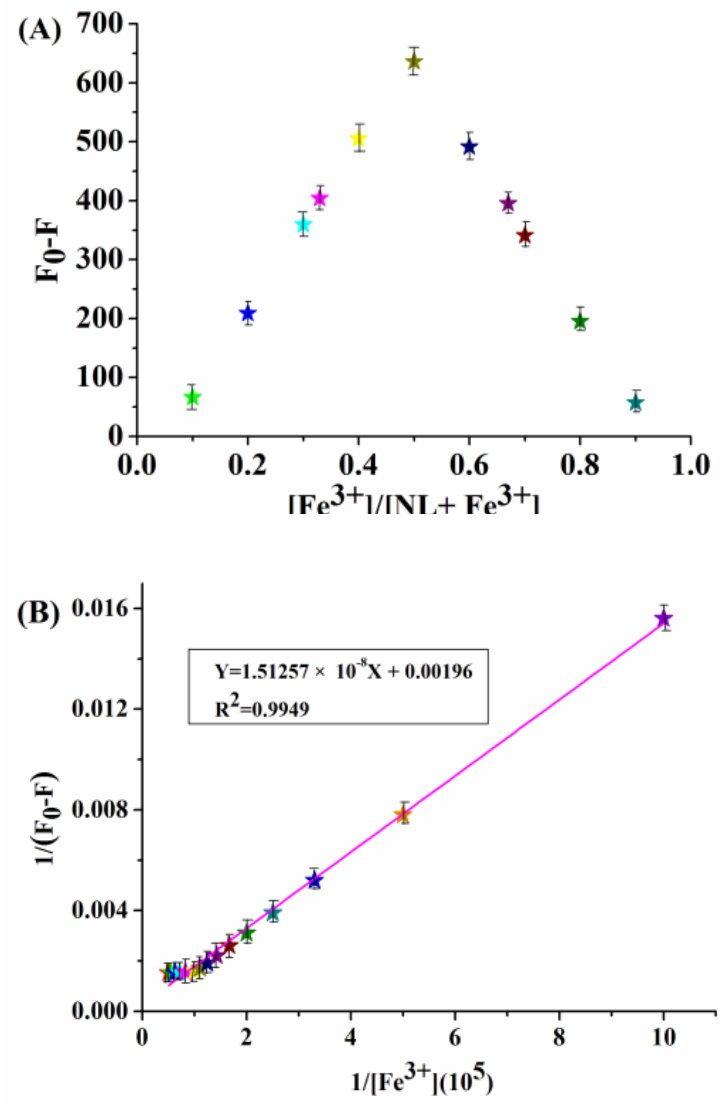

Figure 2. (**A**) The Job's plot of the reaction between **NL** and Fe^{3+} (total concentration was kept at 20 μM). (**B**) The Benesi-Hildebrand plot of **NL** (10 μM) with Fe^{3+}.

The specific recognition of **NL** for Fe^{3+} was then studied by UV-Vis absorption spectroscopy. As shown in Figure 3A, the ligand **NL** showed a maximum absorption at 412 nm in DMSO/H_2O (2:8/*v*:*v*, pH = 7.2) solution, the UV-Vis absorption of **NL** increased gradually when Fe^{3+} (0–20 μM) was added to **NL** (10 μM). The addition of other cations has a negligible effect on the UV spectrum of **NL** (Figure 3B). The association constant of **NL** with Fe^{3+} by UV-Vis spectroscopy was calculated to be 2.16 × 10^5 M^{-1}(R^2 = 0.9952) (Figure S12). A Job plot by UV-Vis spectroscopy showed that **NL** coordinates to Fe^{3+} to form a complex in 1:1 stoichiometry (Figure S13).

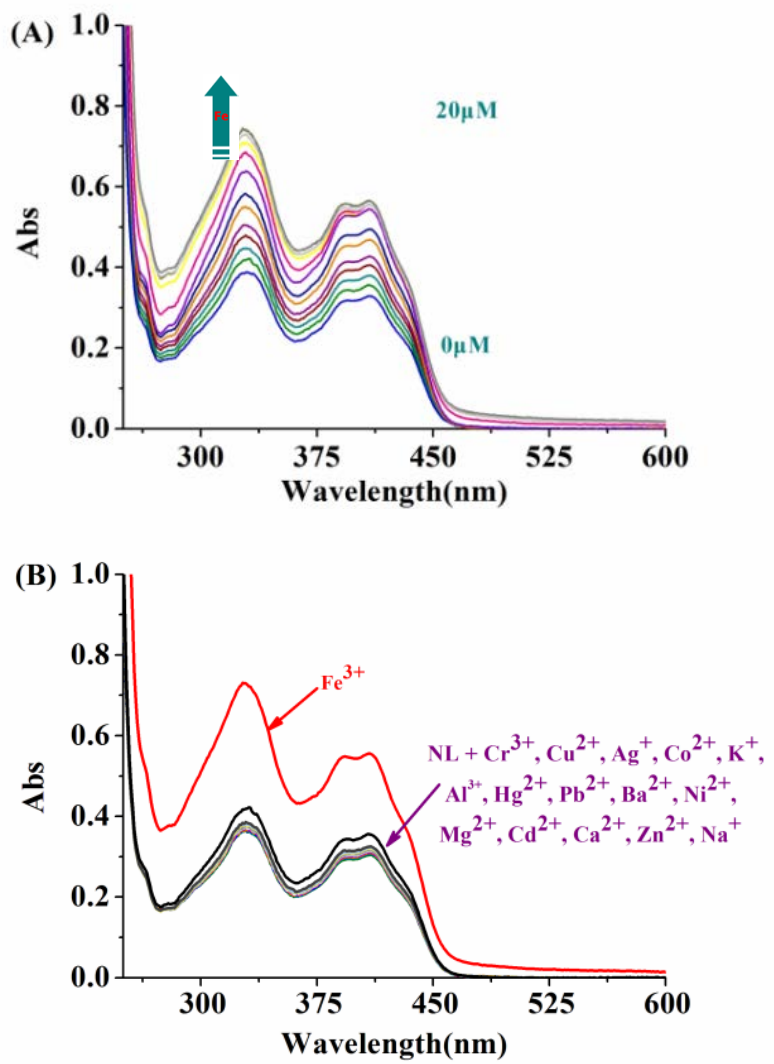

Figure 3. (**A**) UV-Vis titration spectra of **NL** (10 μM) in the presence of different amounts of Fe^{3+} (0–20 μM) in DMSO/H_2O (2:8/*v*:*v*, 20 mM HEPES, pH = 7.2) solution. (**B**) Fluorescence responses of **NL** (10 μM) to different cations (20 μM): Cr^{3+}, Cu^{2+}, Ag^{+}, Co^{2+}, K^{+}, Hg^{2+}, Pb^{2+}, Fe^{3+}, Ba^{2+}, Ni^{2+}, Mg^{2+}, Cd^{2+}, Ca^{2+}, Zn^{2+}, Al^{3+}, and Na^{+}.

3.2. Fluorescence Responses of the NL-Fe^{3+} towards Anions

Due to the coordination property of Fe^{3+}-PPi, **NL**-Fe^{3+} has the potential to be used as a fluorescent chemosensor for PPi recognition by Fe^{3+} displacement approach [27]. The **NL**-Fe^{3+} complex was then synthesized in situ by adding Fe^{3+} (10 μM) into **NL** (10 μM) in DMSO/H_2O (2:8/*v*:*v*, 20 mM HEPES, pH = 7.2) solution. Fluorescence responses of **NL**-Fe^{3+} to various anions were investigated (Figure 4A). It was found that **NL**-Fe^{3+} showed an "off-on" fluorescence response toward PPi (40 μM) selectively, the changes of the emission color of the **NL**-Fe^{3+} chemosensor from colorless to yellow could be observed by the naked eye under UV lamp, while other anions and polyphosphates such as F^{-}, Cl^{-}, Br^{-}, Ac^{-}, HSO_4^{-}, SCN^{-}, HCO_3^{-}, CO_3^{2-}, S^{2-}, NO_2^{-}, SO_4^{2-}, AMP, ADP, ATP, and phosphate (Pi) had no significant effect on the fluorescence intensity of **NL**-Fe^{3+}. This may be attributed to the strong complexation between PPi and Fe^{3+}, which releases **NL** from the **NL**-Fe^{3+} and restores the fluorescence in the presence of PPi. Therefore, **NL**-Fe^{3+} can be used as a selective sensor to detect PPi in aqueous solution.

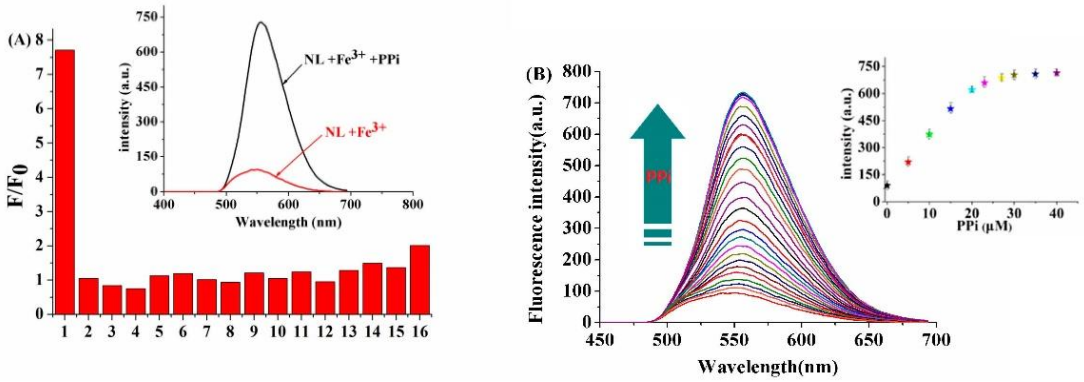

Figure 4. (**A**) Fluorescence responses of **NL**-Fe^{3+} (10 μM) towards various anionic analytes (40 μM): (1) PPi (2) NO_2^-, (3) S^{2-}, (4) F^-, (5) SCN^-, (6) Ac^-, (7) HCO_3^-, (8) HSO_4^-, (9) CO_3^{2-}, (10) Cl^-, (11) Br^-, (12) SO_4^{2-}, (13) AMP, (14) ADP, (15) ATP, (16) Pi. (**B**) Fluorescence spectra of **NL**-Fe^{3+} (10 μM) for different amounts of PPi (0–40 μM) in DMSO/H_2O (2:8/*v*:*v*, 20 mM HEPES, pH = 7.2) solution. Inset: Relationship between the fluorescence intensity of **NL**-Fe^{3+} and concentration of PPi.

One of the important indicators of sensor performance is its high selectivity toward the analyte over other competitive species. The selectivity of **NL**-Fe^{3+} toward PPi in the presence of different anions and polyphosphates was investigated. As shown in Figure S14, upon the addition of 4 equiv. of PPi to the solution of **NL**-Fe^{3+} containing other anions and polyphosphates, the competitive anions and polyphosphate species did not lead to any significant interference, which indicates the high selectivity of **NL**-Fe^{3+} to PPi under the interference of competitive anions.

To further investigate the recognition performance of **NL**-Fe^{3+} toward PPi, fluorescence titration of **NL**-Fe^{3+} with different concentrations of PPi was performed in HEPES buffer solution. As shown in Figure 4B, upon addition of increasing concentrations of PPi to **NL**-Fe^{3+}, the fluorescence intensity of **NL**-Fe^{3+} increased gradually and reached the maximum when 3 equiv. of PPi were added, which is the same as the fluorescence intensity of **NL** (Figure S15), showing the full release of Fe^{3+} by PPi. The detection limit of **NL**-Fe^{3+} for PPi was calculated to be 1.45×10^{-8} M (R^2 = 0.9978) (Figure S16), indicating that **NL**-Fe^{3+} can identify PPi sensitively in buffer solution, and the decomplexation constant of **NL**-Fe^{3+} toward PPi was calculated to be 6.41×10^{10} M^{-1} (R^2 = 0.9946) (Figure S17).

Regeneration is also an important factor to evaluate the performance of a fluorescent chemosensor. The fluorescence spectra of **NL**-Fe^{3+} (10 μM) were observed by adding PPi (30 μM) and Fe^{3+}(10 μM) alternately in DMSO/H_2O (2:8/*v*:*v*, 20 mM HEPES, pH = 7.2) solution, as shown in Figure 5. The reversible fluorescence transformation of **NL**-Fe^{3+} could be repeated more than 5 times, suggesting that **NL** can be used as a reversible fluorescent chemosensor for detecting PPi.

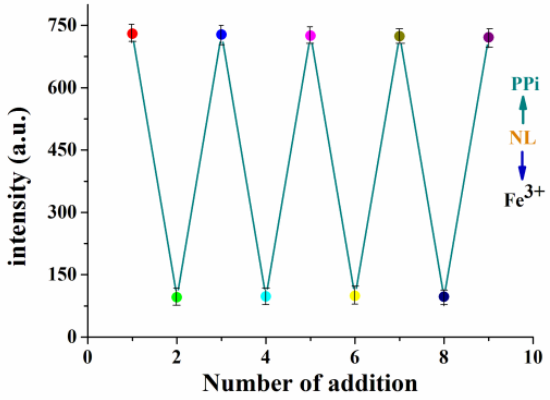

Figure 5. Fluorescence spectral changes of **NL** (10 μM) upon the alternate addition of Fe^{3+} (10 μM) and PPi (30 μM) in HEPES buffer.

The fluorescence response time of **NL**-Fe^{3+} to PPi was further investigated. As shown in Figure S18, significant fluorescence enhancement was observed within 60 s, indicating that **NL**-Fe^{3+} could be used as a fluorescent probe for real-time detection of PPi.

3.3. Ultraviolet Spectrum Responses of the NL-Fe^{3+} towards Anions

The recognition response of **NL**-Fe^{3+} ensemble towards PPi was studied by UV-Vis absorption spectroscopy. As shown in Figure 6A, with the increase of PPi (0–40 μM), the intensity of **NL**-Fe^{3+} decreased gradually and was completely consistent with that of free chemosensor **NL**, which indicates that the sensor **NL** is recyclable. In addition, the addition of other anions and polyphosphates such as F^-, Cl^-, Br^-, Ac^-, HSO_4^-, SCN^-, HCO_3^-, CO_3^{2-}, S^{2-}, NO_2^-, SO_4^{2-}, AMP, ADP, ATP, and phosphate (Pi) had no effect on the absorption spectrum of the **NL**-Fe^{3+} ensemble (Figure 6B), suggesting the high selectivity of **NL**-Fe^{3+} towards PPi, and the decomplexation constant of **NL**-Fe^{3+} toward PPi by UV-Vis titration was calculated to be 6.23×10^{10} M^{-1} (R^2 = 0.9918) (Figure S19).

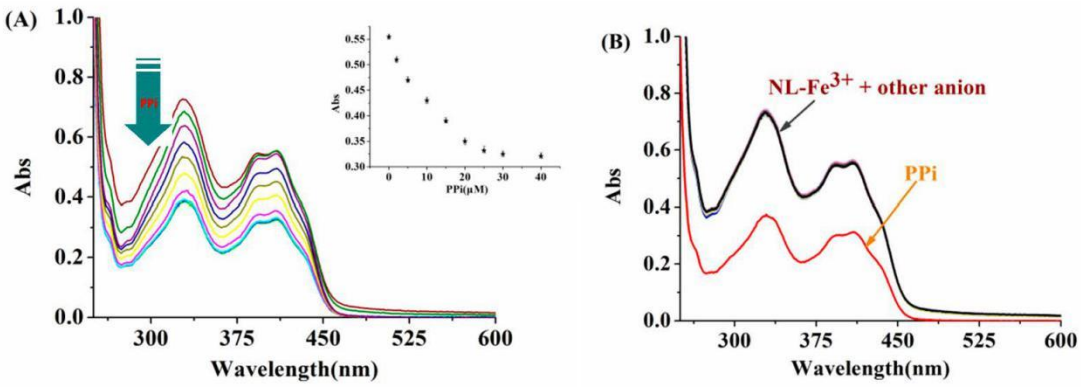

Figure 6. (**A**) UV-Vis spectrum of **NL**-Fe^{3+} (10 μM) toward different amounts of PPi (0–40 μM) in DMSO/H_2O (2:8/*v*:*v*, 20 mM HEPES, pH = 7.2) solution. (**B**) UV-Vis spectrum of **NL**-Fe^{3+} (10 μM) towards various anionic analytes (40 μM): F^-, Cl^-, Br^-, Ac^-, HSO_4^-, SCN^-, HCO_3^-, CO_3^{2-}, S^{2-}, NO_2^-, SO_4^{2-}, AMP, ADP, ATP, PPi, and Pi.

3.4. Effects of pH

The effects of pH value on the fluorescence of **NL** and **NL**-Fe^{3+} were studied. As shown in Figure S20, the fluorescence of **NL**-Fe^{3+} is almost completely quenched at pH 5–10 in DMSO/H_2O (2:8/*v*:*v*, 20 mM HEPES) solution, the strong fluorescence was observed when pyrophosphate was added to the **NL**-Fe^{3+} complex, indicating that **NL**-Fe^{3+} complex is suitable for the recognition of PPi under physiological conditions.

3.5. The Plausible Mechanism of NL towards Fe^{3+} and PPi

The displacement strategy for PPi detection was further validated by the results of MS spectroscopy studies. MS spectra of **NL** showed a molecular-ion peak [**NL**+H^+]$^+$ at m/z 373.11879 (Figure S3). After adding Fe^{3+} into the **NL** solution, the peak generated at m/z 498.94286 was attributed to [**NL**+Fe^{3+}+2Cl^-]$^+$ (Figure S7). This evidence supported the formation of the **NL**-Fe^{3+} ensemble convincingly. Further addition of PPi to the generated **NL**-Fe^{3+}, the MS generated a molecular-ion peak at m/z 373.11883 again (Figure S8), which proves that PPi promotes the release of Fe^{3+} from **NL**-Fe^{3+} complex and results in the restore of ligand **NL**.

Therefore, the reasonable complexion mode of **NL** and Fe^{3+} was proposed according to the above analysis results (Scheme 2). The results showed that Fe^{3+} chelates with the N atom of imino, O atom of hydroxy in naphthol as well as O atom of hydroxy in coumarin. The chelation pattern was confirmed by DFT calculations at the level of B3LYP using 6-31G (d,p) basis set for **NL** and LANL2DZ basis set for **NL**-Fe^{3+} complex using Gaussian 09 program. The configurations of **NL** and **NL**-Fe^{3+} complex and their corresponding energy levels of HOMO and LUMO molecular orbitals were depicted (Figure 7), the HOMO

was distributed on the naphthalene ring of **NL**, and LUMO was distributed on the whole molecule of **NL**. Meanwhile, the π electrons in HOMO orbitals of **NL**-Fe^{3+} complex were distributed on the coumarin. The LUMO was distributed on the complexation part between the heteroatom and the iron in **NL**-Fe^{3+}. The HOMO-LUMO energy gaps of **NL** and **NL**-Fe^{3+} were 0.11 eV and 0.03 eV, showing that the combination of Fe^{3+} and **NL** reduces the HOMO-LUMO energy gap of **NL**-Fe^{3+} and makes the system more stable.

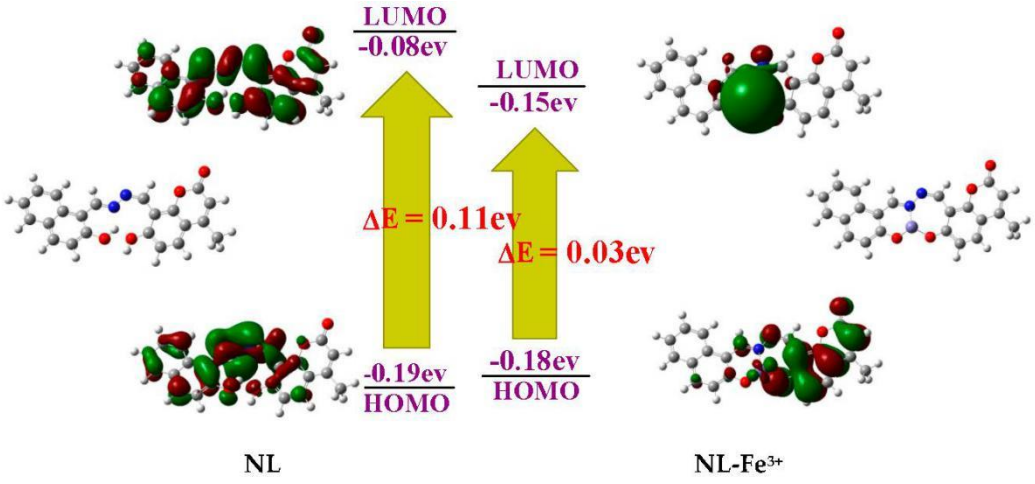

Figure 7. HOMO and LUMO energies of **NL** and **NL**-Fe^{3+} complexes.

3.6. Fluorescence Imaging of Intracellular PPi

The reduction activity of methyl thiazolyl tetrazolium (MTT[3-(4,5-dimethylthiazol-2-yl)-2,5-diphenyltetra-zoliumbromide]) assay was used to determine the cytotoxicity of **NL** in Hep G2 cells. As shown in Figure S21, when **NL** (2–16 μM) were incubated with Hep G2 cells at 37 °C for 24 h, no significant change in the proliferation of Hep G2 cells was observed, and the cell viability remained above 90% after 24 h incubation with **NL**, which indicated that **NL** exhibited low cytotoxicity and had good biocompatibility, and could be used for fluorescence imaging of living cells. To investigate the cytotoxicity of **NL**-Fe^{3+} towards Hep G2 cells, the cells were incubated with **NL**-Fe^{3+} (10 μM) for 48 h. The Hep G2 cells were used as the control group. As shown in Figure S22, the survival of Hep G2 cells incubated with **NL**-Fe^{3+}(10 μM) was still above 92% after 48 h.

Due to its high sensitivity and biocompatibility, the potential application of biological imaging of PPi recognition in live Hep G2 cell was investigated. The cells were incubated with the DMSO/H_2O (2:8/*v*:*v*, pH = 7.2) solution of **NL** (10 μM) in a CO_2 incubator for 30 min at 37 °C. The cells were washed 3 times and treated with Fe^{3+}(10 μM) for 20 min, then were incubated with PPi (30 μM) for another 20 min. As expected, Hep G2 cells cultured with **NL** showed strong yellow fluorescence (Figure 8A), while the fluorescence of cells treated with Fe^{3+} was quenched (Figure 8B), suggesting the formation of **NL**-Fe^{3+} complex in the cell. Then, the strong yellow fluorescence of cells was observed after further incubation with PPi (Figure 8C), which indicates that PPi could lead to the recovery of fluorescence by penetrating the living cell membrane and interacting with **NL**-Fe^{3+}. This indicated that the **NL**-Fe^{3+} complex can be used to detect PPi in biological systems.

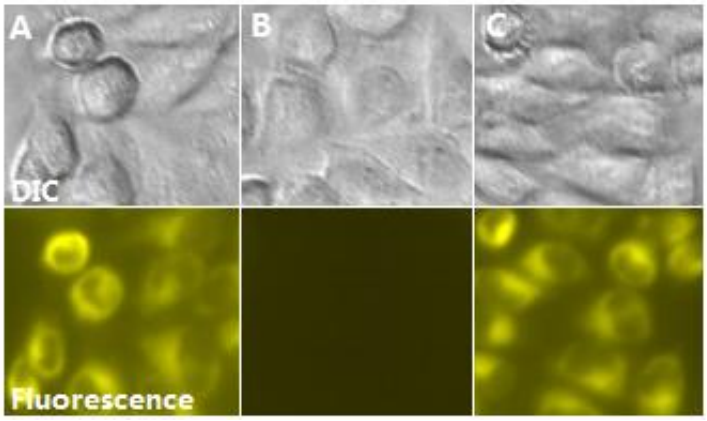

Figure 8. Confocal bright-field (top) and fluorescence (bottom) imaging of Fe^{3+} and PPi in living Hep G2 cells. (**A**) Cells stained with **NL** (10 μM) in a CO_2 incubator for 30 min at 37 °C; (**B**) cells treated with Fe^{3+} (10 μM) for 20 min, (**C**) cells then incubated with PPi (30 μM) for another 20 min.

4. Conclusions

In conclusion, a novel coumarin-Fe^{3+} complex was investigated as fluorescent chemosensor for PPi in DMSO/H_2O (2:8/*v*:*v*, pH = 7.2) solution and biological samples. The chelation of Fe^{3+} with ligand **NL** results in a strong fluorescence quenching. Then, the **NL**-Fe^{3+} complex can be used for PPi recognition by fluorescence "off-on" signaling based on displacement process. The fluorescence "on-off-on"circle can be repeated more than five times when PPi and Fe^{3+} are added alternately, indicating that **NL**-Fe^{3+} is a recyclable chemosensor for detecting PPi. Confocal microscopy showed that **NL**-Fe^{3+} could be utilized for the biological imaging of PPi in Hep G2 cells. In view of the above experimental results, we believe that the designed metal complex provided a flexible strategy for the identification of PPi in biological samples.

Supplementary Materials: The following are available online at https://www.mdpi.com/2227-9040/9/3/48/s1, Figure S1: ^{1}H NMR of **NL**, Figure S2: ^{13}C NMR of **NL**, Figure S3: FT-MS of **NL**, Figure S4: FT-MS of **NL**-Fe^{3+} complex, Figure S5: IR of **NL**-Fe^{3+} complex, Figure S6: UV-Vis of **NL**-Fe^{3+} complex, Figure S7: FT-MS by adding Fe^{3+} into **NL**, Figure S8: FT-MS of **NL**-Fe^{3+} + PPi, Figure S9: Fluorescence spectra of **NL** at different times, Figure S10: Fluorescence intensities of **NL** as a function of Fe^{3+} concentration, Figure S11: Fluorescence response of **NL** to Fe^{3+} in the presence of other common metal ions, Figure S12: The Benesi–Hildebrand of **NL** with Fe^{3+} by UV-Vis spectroscopy, Figure S13: The Job's plot of the reaction between **NL** and Fe^{3+} by UV-Vis spectroscopy, Figure S14: Fluorescence response of **NL**-Fe^{3+} in the presence of various analytes, Figure S15: Fluorescence spectra of **NL**, sequential upon addition of Fe^{3+} and PPi, Figure S16: The linear responses of **NL**-Fe^{3+} versus the concentration of PPi, Figure S17: The decomplexation constant of **NL**-Fe^{3+} toward PPi by fluorescence titration, Figure S18: The fluorescence response time of **NL**-Fe^{3+} in the presence of PPi, Figure S19: The decomplexation constant of **NL**-Fe^{3+} toward PPi by UV-Vis spectroscopy, Figure S20: Fluorescence intensity of **NL**-Fe^{3+} in the absence and presence of PPi at various pH values, Figure S21: Cell viability values assessed using an MTT proliferation test versus incubation concentrations of **NL**, Figure S22: MTT assay of Hep G2 cells treated with **NL**-Fe^{3+}.

Author Contributions: Conceptualization and methodology, W.W. and Y.G.; investigation, H.Z., B.Z., H.L., and Q.L.; writing—original draft preparation, W.W. and Y.G.; writing—review and editing, Y.G.; funding acquisition, B.Z. All authors have read and agreed to the published version of the manuscript.

Funding: This research was funded by National Natural Science Foundation of China (21506106) and the Key Laboratory Project of Liaoning Province (2008S127).

Acknowledgments: We thank Yanan Lei at the School of Chemical and Environmental Engineering, Shanghai Institute of Technology for their help in the cell imaging experiments.

Conflicts of Interest: The authors declare no conflict of interest.

References

1. Lee, G.J.; Marks, J. Intestinal phosphate transport: A therapeutic target in chronic kidney disease and beyond. *Pediatr. Nephrol.* **2015**, *30*, 363–371. [CrossRef]
2. Hansen, N.M.; Felix, R.; Bisaz, S.; Fleisch, H. Aggregation of hydroxyapatite crystals. *Biochim. Biophys. Acta* **1976**, *451*, 549–559. [CrossRef]
3. Florence, W.L.T. Genetics and mechanisms of crystal deposition in calcium pyrophosphate deposition disease. *Curr. Rheumatol. Rep.* **2012**, *14*, 155–160.
4. Costello, J.C.; Rosenthal, A.K.; Kurup, I.V.; Masuda, I.; Medhora, M.; Ryan, L.M. Parallel regulation of extracellular ATP and inorganic pyrophosphate: Roles of growth factors, transduction modulators, and ANK. *Connect. Tissue Res.* **2011**, *52*, 139–146. [CrossRef] [PubMed]
5. Sarkar, D.; Ghosh, P.; Gharami, S.; Kumar Mondal, T.; Murmu, N. A novel coumarin based molecular switch for the sequential detection of Al^{3+} and F^{-}: Application in lung cancer live imagine and construction of logic gate. *Sens. Actuators B Chem.* **2017**, *242*, 338–346. [CrossRef]
6. Rosenthal, A.K.; Ryan, L.M. Calcium pyrophosphate deposition disease. *N. Engl. J. Med.* **2016**, *374*, 2575–2584. [CrossRef]
7. Yang, X.F.; Xie, L.J.; Ning, R.; Gong, X.Q.; Liu, Z.; Li, Y.X.; Zheng, L.Y.; Zhang, G.G.; Gao, B.; Cui, Y.; et al. A diketopyrrolopyrrole-based near-infrared sensor for selective recognition of fluoride ions. *Sens. Actuators B Chem.* **2015**, *210*, 784–794. [CrossRef]
8. Yasuhiro, S.; Rikako, N.; Shunsuke, T.; Chiharu, Y.; Takayuki, H. A naphthalimide-sulfonylhydrazine conjugate as a fluorescent chemodosimeter for hypochlorite. *Chemosensors* **2020**, *8*, 123–135.
9. Miao, R.; Zheng, Q.Y.; Chen, C.F.; Huang, Z.T. A novel calix [4] arene fluorescent receptor for selective recognition of acetate anion. *Tetrahedron Lett.* **2005**, *46*, 2155–2158. [CrossRef]
10. Kumar, R.; Srivastava, A. Anion binding-induced white light emission using a water-tolerant fluorescent molecular tweezer. *Chem. Eur. J.* **2016**, *22*, 3224–3229. [CrossRef]
11. Hu, Z.Q.; Wang, X.M.; Feng, Y.C.; Ding, L.; Li, M.; Lin, C.S. A novel colorimetric and fluorescent chemosensor for acetate ions in aqueous media based on a rhodamine 6G-phenylurea conjugate in the presence of Fe(III) ions. *Chem. Commun.* **2011**, *47*, 1622–1624. [CrossRef]
12. Bhalla, V.; Vij, V.; Kumar, M.; Sharma, P.R.; Kaur, T. Recognition of adenosine monophosphate and $H_2PO_4^{-}$ using zinc ensemble of new hexaphenylbenzene derivative: Potential bioprobe and multichannel keypad system. *Org. Lett.* **2012**, *14*, 1012–1015. [CrossRef]
13. Nadella, S.; Sahoo, J.; Subramanian, P.S.; Sahu, A.; Mishra, S.; Albrecht, M. Sensing of phosphates by using luminescent EuIII and TbIII complexes: Application to the microalgal cell Chlorella vulgaris. *Chem. Eur. J.* **2014**, *20*, 6047–6053. [CrossRef]
14. Ganjali, M.R.; Hosseini, M.; Memari, Z.; Faridbod, F.; Norouzi, P.; Goldooz, H.; Badiei, A. Selective recognition of monohydrogen phosphate by fluorescence enhancement of a new cerium complex. *Anal. Chim. Acta* **2011**, *708*, 107–110. [CrossRef]
15. Zhang, M.; Lu, W.; Zhou, J.; Du, G.; Jiang, L.; Ling, J.; Shen, Z. A simple and effective fluorescent chemosensor for the cascade recognition of Zn^{2+} and $H2PO4^{-}$ ions in protic media. *Tetrahedron* **2014**, *70*, 1011–1015. [CrossRef]
16. Rao, A.S.; Singha, S.; Choi, W.; Ahn, K.H. Studies on acedan-based mononuclear zinc complexes toward selective fluorescent probes for pyrophosphate. *Org. Biomol. Chem.* **2012**, *10*, 8410–8417. [CrossRef] [PubMed]
17. Jiao, S.Y.; Li, K.; Zhang, W.; Liu, Y.H.; Huang, Z.; Yu, X.Q. Cd(II)-terpyridine-based complex as a ratiometric fluorescent probe for pyrophosphate detection in solution and as an imaging agent in living cells. *Dalton Trans.* **2015**, *44*, 1358–1365. [CrossRef] [PubMed]
18. Anbu, S.; Kamalraj, S.; Paul, A.; Jayabaskaran, C.; Pombeiro, A.J.L. The phenanthroimidazole-based dizinc (II) complex as a fluorescent probe for the pyrophosphate ion as generated in polymerase chain reactions and pyrosequencing. *Dalton Trans.* **2015**, *44*, 3930–3933. [PubMed]
19. Roy, B.; Rao, A.S.; Ahn, K.H. Mononuclear Zn(II) and Cu(II) complexes of a hydroxynaphthalene-derived dipicolylamine: Fluorescent sensing behaviours toward pyrophosphate ions. *Org. Biomol. Chem.* **2011**, *9*, 7774–7779. [CrossRef] [PubMed]
20. Wang, W.; Wu, J.; Liu, Q.L.; Gao, Y.; Liu, H.M.; Zhao, B. A highly selective coumarin-based chemosensor for the sequential detection of Fe^{3+} and pyrophosphate and its application in living cell imaging. *Tetrahedron Lett.* **2018**, *59*, 1860–1865. [CrossRef]
21. Bender, D.R.; Kanne, D.; Frazier, J.D.; Rapoport, H. Synthesis and Derivitization of 8-Acetylpsoralens. Acetyl Migrations during Claisen Rearrangement. *J. Org. Chem.* **1983**, *48*, 2709–2719.
22. Wang, W.; Wu, M.; Liu, H.M.; Liu, Q.L.; Gao, Y. A novel on-off-on fluorescent chemosensor for relay detection of Fe^{3+} and PPi in aqueous solution and living cells. *Tetrahedron Lett.* **2019**, *60*, 1631–1635. [CrossRef]
23. Benesi, H.A.; Hildebrand, J.H. A spectrophotometric investigation of the interaction of iodine with aromatic hydrocarbons. *J. Am. Chem. Soc.* **1949**, *71*, 2703–2707. [CrossRef]
24. Beneto, A.J.; Thiagarajan, V.; Siva, A. A tunable ratiometric pH sensor based on phenanthro [9, 10–d] imidazole covalently linked with vinylpyridine. *RSC Adv.* **2015**, *83*, 67849–67852. [CrossRef]
25. Yan, L.Q.; Ma, Y.; Cui, M.F.; Qi, Z.J. A novel coumarin-based fluorescence chemosensor containing L-histidine for aluminium(III) ions in aqueous solution. *Anal. Methods* **2015**, *7*, 6133–6138. [CrossRef]
26. Job, P. Formation and Stability of Inorganic Complexes in Solution. *Ann. Chim.* **1928**, *9*, 113–203.
27. Zhang, R.; Song, B.; Dai, Z.; Ye, Z.; Xiao, Y.; Liu, Y.; Yuan, J. Highly sensitive and selective phosphorescent chemosensors for hypochlorous acid based on ruthenium(II) complexes. *Biosens. Bioelectron.* **2013**, *50*, 1–7. [CrossRef]